LA-UR -90-4208

CONF-901267--1

Received by OSTI

JAN 04 1991

Los Alamos National Laboratory is operated by the University of California for the United States Department of Energy under contract W-7405-ENG-36

LA-UR--90-4208

DE91 005734

TITLE: SHOCK-WAVE EQUATION-OF-STATE STUDIES AT LOS ALAMOS

AUTHOR(S) C(HARLES) E. MORRIS, M-6

SUBMITTED TO SHOCK SYMPOSIUM, DECEMBER 11-12, 1990, TOKYO, JAPAN

DISCLAIMER

MASTER

Los Alamos Los Alamos National Laboratory
Los Alamos, New Mexico 87545

SHOCK-WAVE EQUATION-OF-STATE STUDIES AT LOS ALAMOS*

Charles E. Morris
Los Alamos National Laboratory
Los Alamos, New Mexico, USA 87545

Abstract

A history of the shock-wave equation-of-state (EOS) studies at Los Alamos is given. Particular emphasis is placed on the pioneering research in the 1950s where many of the experimental techniques and methods of analysis were developed, which we now take for granted. A brief review of shock-wave physics is given, which illustrates important hydrodynamic and thermodynamic concepts. Recent studies on the EOS of Ti are presented with emphasis on the α-to-ω phase transition. VISAR wave profiles on polycrystalline Ni and single-crystal Ni are presented to determine the strengths of these materials at pressure. Low-density polystyrene foam Hugoniot experiments are described and results analyzed.

HISTORICAL EQUATION-OF-STATE REVIEW

EOS research at Los Alamos started with the Manhattan Project. It was immediately clear that high-pressure/high-temperature EOS were needed to model nuclear weapon systems. During World War II, very little time was available for research because of the crash program to develop a nuclear weapon. During the years from 1946 to 1950 a research program was started that generally involved the use of electrical contactor pins to monitor the motion of metal plates accelerated by high explosives. The history of this research has been described by J. W. Taylor.[1] The EOS history that I will describe begins with the research done by the Shock Wave Physics Group at Los Alamos. This group is responsible for many of the experimental techniques that we utilize today, along with a prodigious amount of EOS data that has been published in the open literature.

The success of the research program can be credited to several scientists that came into M-6 starting in 1950. They were J. M. Walsh (1950), W. E. Deal (1950), C. M. Fowler (1952), M. H. Rice (1952 as a graduate student), R. G. McQueen (1955), S. P. Marsh (1955), J. N. Fritz (1955 as a graduate student), J. Wackerle (1956), and J. W. Taylor (1957). The vast majority of these people are still actively involved in shock wave physics research.

In 1950 the high-velocity guns we use today were not available. What was available at Los Alamos was the most advanced high-explosive fabrication technology anywhere. There was an in-house capability to fabricate high quality, precision-finished blocks of virtually every practical explosive. They were also able to fabricate plane wave lenses with extreme quality standards. This was the capability that was exploited by Walsh to make the first EOS measurements using the flash-gap technique[2] in 1950. Explosives placed in contact with metal plates could generate shock waves in plates from 1 to 30 GPa. The electrical contactor pins were unreliable for many measurements because they sometimes pretriggered due to shock induced ionization. The pin assemblies were also very tedious to assemble, because a large number of pins were required to define the shape of the input shock wave. Walsh developed the flash-gap technique where an argon flash-gap approximately 0.1 mm thick was placed over the metal surfaces to be monitored. When the shock emerges from the surface, the gas radiates brilliantly and then is rapidly quenched as the plastic surface reacts with the high temperature gas upon shock reflection. This technique was used to measure both shock velocity (u_s) and free surface (u_{fs}) in the samples of interest. The particle velocity (u_p) was calculated using the free-surface approximation $u_p = u_{fs}/2$.

In 1954 the Hugoniots of 27 Metals paper[3] was published with an improved flash gap assembly using the recessed explosive geometry. In this paper, u_p was determined using the impedance matching technique. This advance was important because now the free-surface approximation did not have to be used. A modern version of the flash gap assembly is shown in Fig. 1. The base plate on which the samples were placed was fabricated from a shock wave standard whose Hugoniot and c_0 Hugoniot characteristics were previously determined. Lucite flash gap blocks are placed over and around each sample on the base plate. Shims made of material that effectively excite the flash

* This work was supported by the US Department of Energy.

gap are placed under all flash-gap blocks where necessary to get uniform traces on the photographic record. A gas box is placed over the assembly so argon could be used in the flash gaps. A slit plate with multiple slits for each sample is placed on the top of the gas box. Generally, four slits are used over each sample and their corresponding reference flash-gap blocks. A streak camera was used to record the experimental record. To calculate the transit times through the samples, the shape of the input shock front can be determined from the reference traces. In this manner accurate transit times of the order of a few nanoseconds can be determined from the streak camera records. To get shock velocities accurate to $\pm 1\%$, gap-closure times needed to be taken into account. In each assembly, two samples of the base-plate material are included to determine the shock strength in the base plate. The IM technique (Fig. 2) is based on the observation that pressure and particle velocity are continuous across the base-plate-sample interface. The intersection of the sample shock locus $(P \quad (\rho_s u_s) u_p)$ with the cross curves, either reflected shocks or release curves, from the (u_p, P) state in the base plate determined the particle velocities of the samples. These assemblies greatly simplified the case with which measurements could be made, because now only shock velocities in the samples and base-plate material needed to be measured. Considerable effort was made researching solid-state theory to find an EOS theory suitable for calculating off-Hugoniot states. It was decided the Mie Grüneisen EOS[4] was most appropriate. Given this EOS and the Grüneisen gamma (γ), the appropriate cross curves could be calculated.

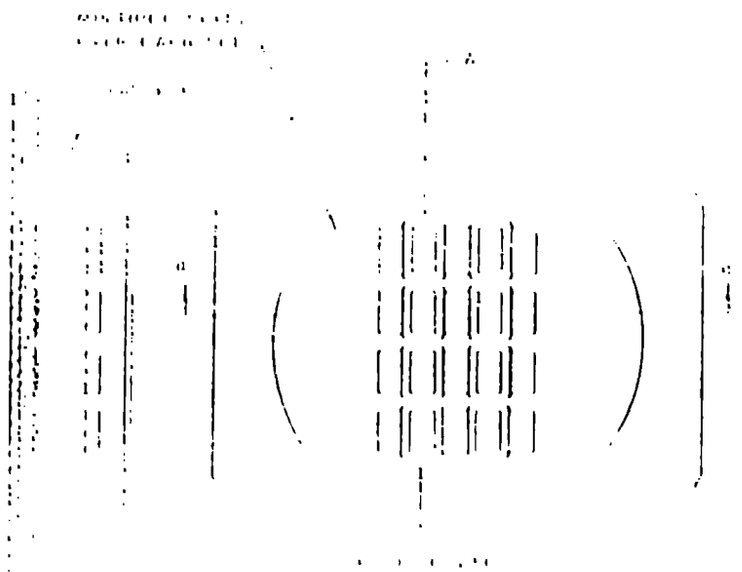

Fig. 1. Flash-gap assembly used to obtain shock wave data with impedance-match technique

The publication of "Compression of Solids by Strong Shock Waves" by M. H. Rice, R. G. McQueen, and J. M. Walsh in 1958 was an important milestone in pressure-shear plate impact research. The shock wave technique and theoretical analysis used in the emerging shock wave physics field. For this contribution, the authors received the first American Physical Society Shock Compression of Condensed Matter Award in 1985. In the publication, the Hugoniot $\rho_0 u_s u_p$ was presented for the first time. The particle velocity wave profile, which was universally used, was first derived by R. G. McQueen when he was plotting experimental data rather than derived data that was conventionally done at that time. Representation of shock wave data in this format provides insight in data interpretation that was not evident in

other presentations. Various models for the Grüneisen gamma were also presented. The experimental procedures developed by Rice, McQueen, and Walsh, and summarized in this publication, were well suited to mass production. Over 500 materials have been studied[6] using the technique.

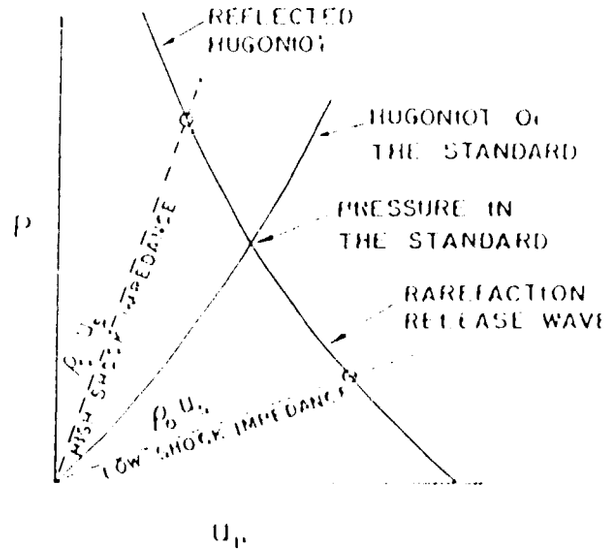

Fig. 2. Schematic for obtaining Hugoniot data using the impedance-match technique.

The in-contact explosive geometry makes use of only the initial HE/base-plate interaction, consequently only modest pressures can be generated. Schreffler and Deal[7] demonstrated that high explosives (HE) could accelerate thin metal plates to high velocities over a few centimeters of travel. This capability was used by McQueen and Marsh in their 19 Metals paper[8] published in 1960 to measure Hugoniots to 200 GPa (2 Mbar). With these HE free-run systems, the Hugoniots could be extended by approximately a factor of four in pressure. The Hugoniots over this expanded pressure range remained linear. These data reinforced the linear u_s-u_p relation as a viable representation of Hugoniot data. It is worthwhile to point out that in a ten-year time span, shock-wave techniques expanded by about two orders of magnitude the range over which EOS information was available. This was truly remarkable.

In the IM technique the base plate is made of a standard whose Hugoniot and cross curves need to be known. For the in-contact geometry only modest pressures were attained (up to 50 GPa), so the calculated cross curves (reflected shock and release isentropes) were only slightly offset from the Hugoniot. Consequently, moderate uncertainties in Grüneisen parameter could be tolerated and still calculate accurate particle velocities. With the use of the free-run explosive systems, much higher pressures were generated. Now the offsets of the calculated cross curves start to become considerably larger. To maintain accurate calculated particle velocities, a thorough characterization of the Grüneisen parameter was needed. To address this problem, a standards characterization program was implemented at Los Alamos.[9,10,11] A standard for the purpose of program is a material whose EOS has been determined that does not use the EOS of some other material. Cu, Fe, and 2024Al have been characterized as standards. Their hugoniots and average Grüneisen parameters $\langle\gamma\rangle$ were experimentally determined.

An experimental assembly[9,10,11] used to make these measurements is given in Fig. 3. The base plate and driver are made of the standard to be studied. The left side of the assembly is used to make shock-velocity measurements, while the right side is used to make driver-velocity measurements. Each set of flash blocks are viewed by four or five slits. The shock velocity is determined by measuring the transit time through two different thicknesses of base plate. The driver velocity is measured through the use of a groove cut into the impact side of the base plate. The measured time offset is related to the difference in velocities between the driver and shock velocities. Even though the system appears quite simple, careful attention is required so that lateral perturbations do not influence transit time measurements. To optimize these measurements, low, intermediate, and high pressure assemblies used grooves of varying depths and base plates of various thicknesses.

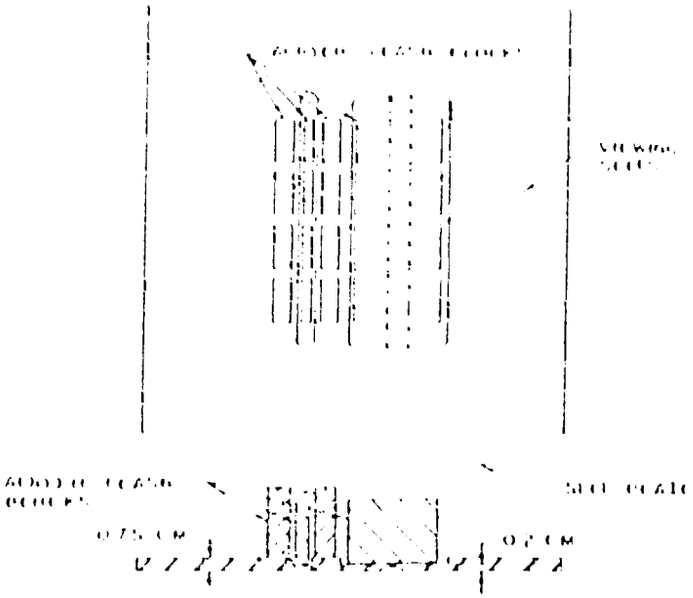

Fig. 3. Target plate for standard's characterization. Left side used to measure shock velocity, right side used to measure impactor velocity

The average Grüneisen parameter $\langle\gamma\rangle$ can be measured using porous samples as shown in Fig. 4. When crystal density and porous samples are shocked to the same volumes, there is pressure offset ΔP due to the difference in the internal energies represented by the cross-hatched area. The average Grüneisen parameter is given by $\langle\gamma\rangle = V\Delta P/\Delta E|_V$. Hugoniot measurements of porous standards of various densities were made using the flash-gap assembly in Fig. 1. Both the base plate and samples were made with the same standard material. On a given shot there were six porous samples of various densities and two of the base-plate material. In Fig. 5 are the porous Hugoniots for 2024Al at crystal density and four porous densities. The solid line through the data points were Hugoniots calculated using the familiar $\rho\gamma = \rho_o\gamma_o$ assumption and the average densities for each porosity. Within the accuracy of the data the $\rho\gamma$ constant assumption fits the data set quite well. The Cu and Fe porous data could also be fitted using the same γ formulation. From these studies it was concluded that the constant $\rho\gamma$ approximation was adequate, if no other data precluded its use.

Over the last decade, sound-speed measurements at pressure have dramatically expanded our knowledge of material behavior. Sound-speed measurements complement Hugoniot data in that they measure derivatives on the EOS surface. Consequently, these measurements can detect small first-order phase transformations and second order phase transformations that are not evident on the Hugoniot. Sound speeds in the liquid state, coupled with Hugoniot data, allow the Grüneisen parameter to be calculated with good precision, a quantity of prime theoretical interest. Because of the nature of how sound velocities are measured, they can be determined with the same precision as shock velocities. To date, sound velocities have been measured on C, Al, Fe, Mo, Ta, W, CsI, La, and Pb.

A technique that is ideally suited to measuring lead characteristics of sound waves at pressure is the optical analyzer[12] developed by R. G. McQueen. An experimental assembly for an explosive shot is shown in Fig. 6. A step wedge target is impacted with a driver of the same material, if possible. However, this is not necessary to make these measurements. Bromoform ($CHBr_3$) liquid is placed on top of the step wedge to function as an optical detector. When a shock propagates in bromoform, it radiates profusely and continues to radiate at a constant level until the release wave from the driver overtakes the leading shock. The radiation from the shock in the bromoform is collected by light pipes that are centered over each step wedge level. Apertures are placed above the step wedge so that the viewing diameter of the light pipe is approximately 1 mm. With this viewing diameter, tilt effects are negligible. Baffles are included in the assembly to prevent cross talk between light pipes. Specially designed Beck photomultiplier circuits[13] are used to optimize the photomultiplier's response so that they have risetimes of the order of 1 ns. Three features of this assembly enable very accurate sound velocities to be made. Usually the wave arrivals in these experiments are smeared out. Because the radiation is proportional to something greater than the fourth power of pressure, the lead characteristic arrival is quite discernible in these experiments. The fact that the sound wave arrival

can be measured at several different levels allows one to plot Δt verses l_T to determine at what target thickness the release wave overtakes the shock wave. Δt in these experiments is the time interval between when the shock enters the bromoform until it is overtaken by the release from the driver. In this manner the hydrodynamic perturbations due to the analyzer are eliminated. Finally, since Δt's are measured at several sample thickness, statistics can be use to get accurate overtake distances in the target. For $\Delta t = 0$,

$$^{l}c/u_s = (R+1)/(R-1) \tag{1}$$

where $R = l_T/l_D$ and $^{l}c = (\rho/\rho_o)c$. In some experiments, velocities ratios $^{l}c/u_s$ of a few 0.1% have been measured.

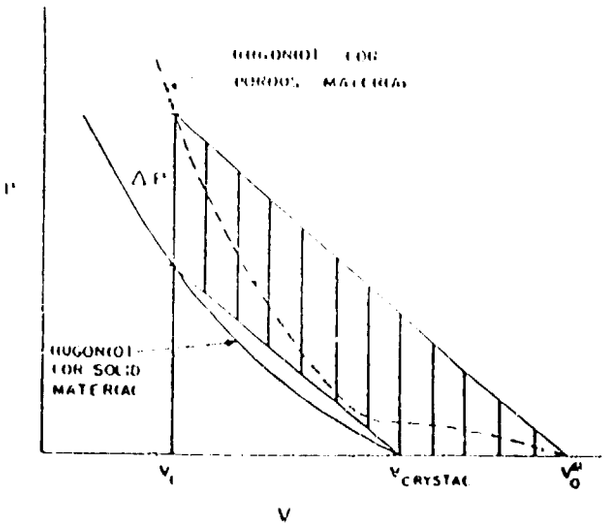

Fig. 4. Schematic illustrating how porous materials are used to measure the Grüneisen parameter.

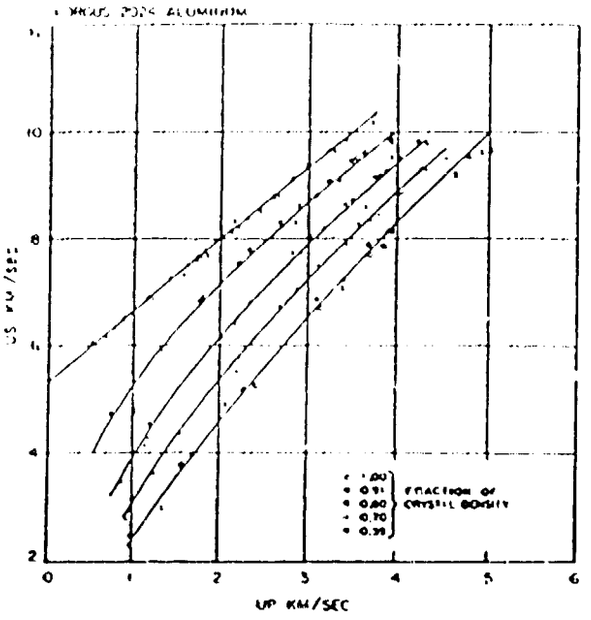

Fig. 5. Shock-Particle velocity for porous 2024Al with 1.00, 0.91, 0.80, 0.70, and 0.59 fractional crystal densities.

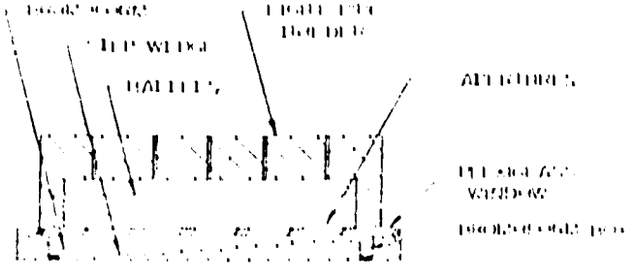

Fig. 6. Optical analyzer target assembly. The assembly is impacted on the bottom surface with a thin driver to measure impactor velocity.

BASIC SHOCK-WAVE PHYSICS RELATIONS

Hugoniot

Consider a shock wave with a steady profile propagating into a material that is at rest. Conservation of mass, momentum, and energy gives the Rankine-Hugoniot equations.

$$(1 - V/V_o) = u_p/u_s \tag{2}$$

$$P - P_o = \rho_o u_s u_p \tag{3}$$

$$E - E_o = u_p^2/2 + P_o V_o u_p/u_s \quad . \tag{4}$$

These equations relate the pressure, P, specific internal energy, E, specific volume, V, behind the shock to those same quantities in front of the shock wave in terms of shock velocity, u_s, and particle velocity, u_p. The initial state parameters represented by P_o, V_o, and E_o are often referred to as the centering point of the Hugoniot. Measurement of any two of the variables (P, V, E, u_s, and u_p) with the above equations is sufficient to determine the remaining variables. Equations (2) and (3) can be combined to give

$$u_s = V_o[(P - P_o)/(V_o - V)]^{1/2} \quad , \tag{5}$$

and

$$u_p = [(P - P_o)(V_o - V)]^{1/2} \quad . \tag{6}$$

Substituting Eqs. (5) and (6) into (4) gives the Hugoniot energy equation

$$E - E_o = (P + P_o)(V_o - V)/2 \quad . \tag{7}$$

The Rankine-Hugoniot relations are the cornerstone of shock-wave physics. They are based on Newton's Laws and the conservation of mass and energy. This allows the absolute measurement of pressure, compression, and internal energy without the use of secondary standards. u_s and u_p can be measured to 1/2%. This enables pressure and compression to be determined to 1%. The Hugoniots measured in the early 1950s differ with our current Hugoniot measurements by about 1%. This was due to a recalibration of our streak cameras with an improved calibration procedure. It is interesting to contrast dynamic measurements with static high-pressure research where high-pressures scales changed by as much as a factor of 2 from the 1950s to the 1970s.

From the energy equation, Eq. (4), it is apparent that there is an equal partition of energy between internal energy ($E - E_o$) and kinetic energy, if the $P_o V_o u_p/u_s$ term is ignored. This is an excellent approximation for all our studies. It is straightforward to show[11,14] that $dP/dV|_H$ and $d^2P/dV^2|_H$ on the Hugoniot are equal to $dP/dV|_S$ and $d^2P/dV^2|_S$ on the isentrope at the Hugoniot centering point. Another interesting characteristic of the Hugoniot is that the entropy increases monotonically with shock strength.

Grüneisen Parameter

The Hugoniot specifies a path on the EOS surface. In order to model other dynamical processes such as reflected shocks and release isentropes, we need to be able to calculate off-Hugoniot states. The thermodynamic variable that allows this calculation to be made is the Grüneisen parameter[15,16] defined as

$$\gamma/V = (\partial P/\partial E)_V = (\partial P/\partial T)_V/C_V \quad . \tag{8}$$

To model the thermal energy of a solid, it is assumed the energy is that of a collection of simple harmonic oscillations that are the normal modes of the crystalline lattice. It will further be assumed the individual mode gammas γ_i are only a function of volume. The summations over the 3n modes of the lattice give

$$\gamma = \sum_i C_{v_i}\gamma_i / \sum_i C_{v_i} \quad , \tag{9}$$

which relates the individual mode gammas γ_i to the macroscopic Grüneisen parameter. The individual γ_i's are defined by

$$\gamma_i = -d\ln\nu_i/d\ln V \tag{10}$$

and the heat capacities of the oscillators have the usual form

$$C_i/k = x^2 e^x/(e^x - 1)^2 \quad . \tag{11}$$

$x_i = h\nu_i/kT \equiv \theta_i/T$, where ν_i is the frequency of the oscillator and θ_i is its characteristic temperature. With this definition of γ, it is evident from Eq. (9) that in general γ is a function of both V and T. Two special cases are worth noting. If all the γ_i's are equal, then $\gamma = \gamma_i = \gamma(V)$. In the high-temperature limit $kT >> h\nu_i$, $C_i = k$, then $\gamma = \Sigma\gamma_i/3n = \gamma(V)$. This is the case for most of the metals studied. This greatly simplifies the calculation of off-Hugoniot states. In this case Eq. (8) can be integrated to give the familiar Mie-Grüneisen EOS[3,5]

$$(P - P_H) = (\gamma/V)(E - E_H) \quad . \tag{12}$$

For materials in their high-temperature limit, Eq. (12) has been quite adequate in modeling their EOS. The Mie-Grüneisen EOS was used for calculating average γ's for porous metals of Cu, Fe, and 2024Al. The familiar

$$\rho\gamma = \rho_o\gamma_o \tag{13}$$

relation was adequate to fit this data. Unless there is specific information to exclude this γ choice, this functional form of γ is usually chosen.

The availability of high-pressure sound-speed data has allowed direct γ determinations along the Hugoniot. A relation[17] that relates sound speeds to γ is

$$\frac{\gamma(V_o - V)}{2V} = \frac{B_H/V - B_S/V}{B_H/V - (P_H - P_o)/(V_o - V)} \tag{14}$$

where $\rho c^2 = -V\,dP_S/dV \equiv B_S$ and $B_H = -V\,dP_H/dV$. This equation is valid for $\gamma(V,T)$ and $\gamma(V)$. γ is proportional to the ratio of the differences in slopes between the Hugoniot and the isentrope and between the Hugoniot slope and chord slope. Only at high pressures is there sufficient differences in slopes to make meaningful γ determinations. For example, a 1% sound-speed measurement in OFHC Cu at 25 GPa determines γ to 52%, 125 GPa, —, 9%. For polymers, which are much more compressible at low pressures, a 1% sound-speed measurement in PTFE[16] at 40 GPa results in a 3% γ determination. The majority of sound speed measurements have been made on metals. As a consequence, the linear $\rho\gamma$ relationship has usually been quite adequate, in agreement with the porous metal measurements. However, for PTFE (Teflon) the assumption $\gamma = \gamma(V)$ was not valid and a dramatically different γ dependence was observed. The important point to remember is that the γ formulation in Eq. 13 applies to a broad class of materials; however, there are exceptions where this formulation does not apply.

Linear u_s - u_p Relation

Previously, it was mentioned that many materials can be adequately represented by a linear Hugoniot.

$$u_s = c_o + s\,u_p \tag{15}$$

c_o is the zero-pressure intercept and s is the slope. c_o is the zero-pressure shock velocity and should be equal to the zero-pressure bulk sound velocity C_B, because of common slopes on the Hugoniot and isentrope. For polycrystalline samples

$$C_B^2 = C_L^2 - 4/3C_s^2 \quad , \tag{16}$$

where C_L and C_s are the longitudinal and shear elastic wave velocities. In most instances the agreement of the shock wave intercept, c_o, and C_B is within experimental accuracy.[5,6] The appropriateness and adequacy of Eq. (15) has been examined by Ruoff[14] and Jeanloz and Grover.[17] Ruoff[14] and McQueen[6] have shown that the Hugoniot slope is related to the pressure derivative of the isentropic bulk modulus by the relation

$$(dB_s/dP)_{P=P_o} = 4s - 1 \tag{17}$$

The quantity is difficult to measure statically with good accuracy. However, there is a general interest in dB_s/dP, because several EOS models[17] use this variable. It is important to point out that there

are several instances when the linear u_s-u_p relation breaks down. Solids with porosity,[9,10,11] large elastic waves, phase transformations, or van der Waals bonding[16] all exhibit departures from this linear behavior.

Using Eq. (15) the Hugoniot of materials centered at zero pressure can be described with three parameters, P_o, c_o, and s. The shock wave locus can be found for any pair of variables using the Rankine-Hugoniot Eqs. (2)–(4). By defining the sample compression as

$$\eta = 1 - V/V_o \tag{18}$$

the conservation of mass Eq. (2) becomes

$$\eta = u_p/u_s \quad . \tag{19}$$

From Eqs. (3), (15), and (19) the $P_H - \eta$ relations can be derived

$$P_H = \rho_o c_o^2 \eta/(1 - s\eta)^2 \tag{20}$$

$$dP_H/d\eta = \rho_o c_o^2 (1 + s\eta)/(1 - s\eta)^3 \quad . \tag{21}$$

It is evident from Eqs. (20) and (21) that the asymptotic compression on the Hugoniot is

$$\eta_A = 1/s \quad . \tag{22}$$

For 2024Al and Cu, their respective Hugoniot slopes are 1.338 and 1.489. This implies 2024Al and Cu have maximum compressions, respectively, of 75% and 67%.

SHOCK WAVE EQUATION OF STATE OF TITANIUM

VISAR wave profile measurements were made on A-70 Ti (commercially pure, 99%) to study the α-to-ω transformation and the "apparent" phase transition at 17.5 GPa. The previous Hugoniot measurements using flash-gap experimentation were made with commercial pure Ti with approximately the same composition as the A-70 Ti. No evidence of a phase transition was observed up to 35 GPa. The observed wave profiles consisted of a large elastic wave (1.8 GPa) followed by a bulk wave with a few nanoseconds risetime. The VISAR data smoothly extrapolated into the higher pressure flash-gap data above the kink in the u_s-u_p curve. The VISAR data conclusively showed the kink in the curve was an artifact of the flash-gap experimentation. The probable reason for kink in the flash-gap Hugoniot data was that the large elastic wave prematurely closed the flash gaps. This interpretation is consistent with the shape of the low-pressure portion of u_s-u_p curve. One would expect greatest departure from a linear extrapolation at low pressures and gradually diminishing to zero at a velocity slightly greater than the measured longitudinal velocity at zero pressure. Two-stage light gas gun data were used to extend the pressure range from 110 GPa to 260 GPa. The high-pressure gun data fell on a linear extrapolation to high pressure of the VISAR/flash-gap Hugoniot data.

VISAR measurements were also made on Ti (electrolytic grade, 99.95%) from 6 to 22 GPa. Below 10 GPa a classic elastic-plastic two-wave structure was observed. At 15 GPa a three-wave structure (elastic plus two bulk waves) was observed, characteristic of a high-pressure first-order phase transition (Fig. 7). The best estimate of the transition pressure is 10.4 GPa. Several shots were fired at this pressure. All shots reproduced this three-wave structure. Shots were also fired at different sample thicknesses to evaluate the kinetics of the transition. At 22 GPa only a two-wave elastic-plastic structure was observed, indicating the bulk transition wave had already overtaken the initial bulk shock. In other words, the Ti wave profiles are consistent with a material undergoing a first-order phase transition at 10.4 GPa with a small volume change.

Shock-recovery experiments were done to complement the VISAR studies using the soft recovery techniques of Gray.[18] Recovered A70-Ti samples shocked to 13 GPa showed no ω phase using TEM, x ray, or neutron scattering measurements. However, Ti, when shocked to 11 GPa, showed the ω phase using all three techniques. From the neutron-scattering measurements the estimated volume fraction of retained ω phase is 28%. In summary, the shock recovery experiments of G. T. Gray III are in agreement with the VISAR wave profile data.

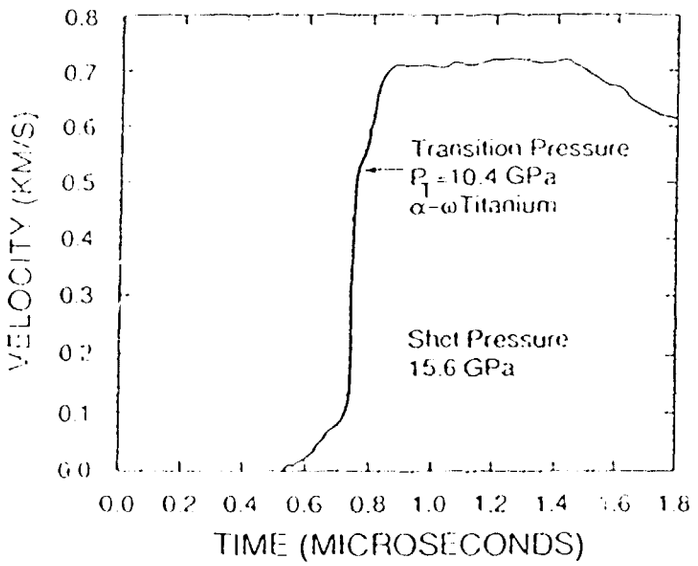

Fig. 7. VISAR wave profile of Ti showing the α-ω transition.

HIGH PRESSURE RELEASE WAVE PROFILES IN SINGLE CRYSTAL AND POLYCRYSTALLINE NICKEL

Nickel (Ni) was chosen as the material to be studied, because it is elastically very anistropic. For example, at ambient conditions the longitudinal velocities of the [100] crystal, the polycrystal, and the [111] crystal are, respectively, 5.28 km/s, 5.76 km/s, and 6.28 km/s. On a relative basis, the velocities are 1, 1.09, and 1.19. At high pressure, if single-crystal structure is preserved, one would expect measurably different release velocities for [100] single-crystal and polycrystal samples. Also, from the shape and amplitude of the release waves, the shear strength at pressure can be calculated.

Symmetric impact experiments were made on [100] single crystals and polycrystalline Ni samples, which had LiF windows. A VISAR was used to make wave profile measurements with 1-ns resolution and 1% particle velocity measurements. The measurements were made at 45 GPa, principally to overdrive the longitudinal elastic wave in the polycrystalline sample, so that a simple centered release wave would be generated at the impactor free surface. This allowed the fine structure of the release waves to be examined and accurate calculations of the release wave velocities and the shear strength of the material at pressure. The measured wave profiles for polycrystalline Ni at 45 GPa and [100] single-crystal Ni at 44 GPa are given in Figs. 8 and 9, respectively.

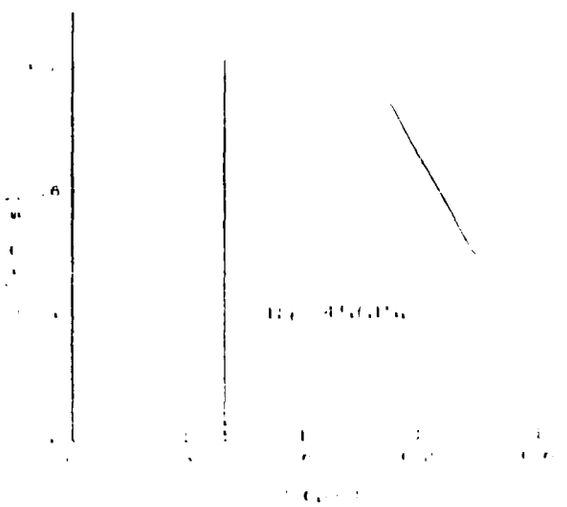

Fig. 8. Quasi-elastic release in polycrystalline Ni from symmetric impact at 45 GPa.

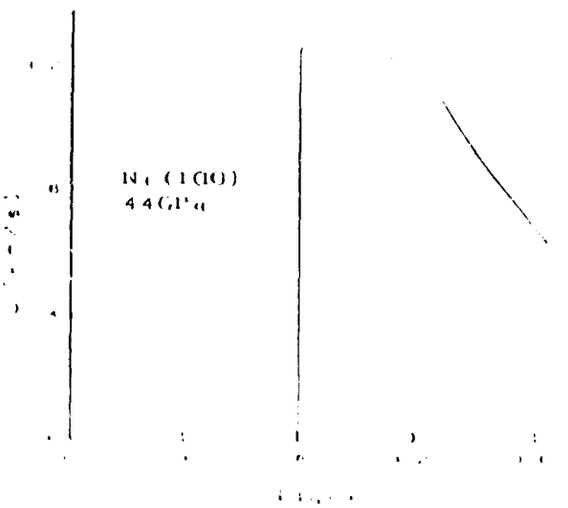

Fig. 9. Quasi-elastic release in [100] single-crystal Ni from symmetric impact at 44 GPa.

The measured release wave velocities at pressure for [100] single crystal and polycrystal are 6.80 km/s and 7.42 km/s. The polycrystal velocity is 9% larger than the [100] single-crystal velocity, which is the same velocity ratio measured at ambient conditions. It is evident that each sample propagates different longitudinal wave velocities. This is a strong indication that the crystal structure, either single crystal or polycrystal, is preserved in spite of the large defect concentration generated by the shock and manifested in the smeared-out quasi-elastic release. These experiments suggest it is appropriate to envision a shock as a highly-coordinated movement of atoms on a subnanosecond time scale that is not chaotic. For the [100] single-crystal sample, a single-crystal lattice with defects is present after the shocking, not microstructure characteristic of a polycrystalline sample.

Both wave profiles show a quasi-elastic release. There is no indication of an ideal elastic-plastic flow, even in the [100] single crystal. The change in the shear stress upon unloading is given by[19]

$$\tau_c + \tau_o = \frac{3}{4}\rho_o \int_{\eta_o}^{\eta_1} ({}^{l}c^2 - {}^{l}c_B^2)\,d\eta \tag{23}$$

where τ_o and τ_c are the shear stress in the shocked state and on the lower yield surface, ${}^{l}c$ is the Lagrangian release wave velocity, and ${}^{l}c_B$ is the Lagrangian bulk wave velocity. The shear stress is defined by the relation

$$\tau = (\sigma_n - \sigma_t)/2 \tag{24}$$

where σ_n and σ_t are the normal and tangential stresses. It is not immediately obvious, but this equation is valid for both polycrystal and [100] single-crystal experiments. The calculated value for $\tau_c + \tau_o$ for [100] single crystal is 0.76 GPa, for the polycrystal 0.92 GPa. The polycrystal has a 21% larger value for $\tau_c + \tau_o$. If τ_o, the shear stress in the shocked state, lies on the upper yield surface, then $\tau_o - \tau_c$, and the shear strength, τ_c, of the material in the shocked state is simply 1/2 the values listed above. It is evident from these calculations that the polycrystal has a larger shear strength, but for the most part their strengths are quite comparable.

To illustrate the essential features of the quasi-elastic release, a simple linear elastic theory[20] was used to relate the actual release wave velocity to the elastic constants of the material and the amount of plastic strain γ occurring during the quasi-elastic release. It can be shown from linear elastic theory that

$$c^2 = C_L^2 - \frac{4}{3}C_S^2(2\,d\gamma/d\eta) \tag{25}$$

for an isotropic solid, and for [100] cubic crystal

$$\rho c^2 = C_{11} - \frac{4}{3}\left[\frac{C_{11} - C_{12}}{2}\right](2\,d\gamma/d\eta) \tag{26}$$

$d\gamma/d\eta$ is the ratio of plastic strain increment $d\gamma$ to total strain increment $d\eta$. For elastic response $d\gamma/d\eta = 0$ the above equations give c equal to the elastic longitudinal velocity. On the yield surface $d\gamma/d\eta = 1/2$, the equations then give c equal to the bulk wave velocity. For the quasi-elastic release in [110] Ni, the Lagrangian wave velocity is given in Fig. 10 and the calculated values of $2\,d\gamma/d\eta$ are given in Fig. 11. It is immediately obvious that the quasi-elastic release is a result of plastic flow occurring immediately in the elastic release rather than when the release reaches the yield surface on which $\tau_c = (\sigma_n - \sigma_t)/2$, as would have occurred in the ideal elastic-plastic model.

Both Ni wave profiles show similar quasi-elastic features, mainly a smeared out release rather than an ideal elastic-plastic response. This suggests the quasi-elastic character is not due to the heterogeneous nature of a polycrystalline aggregate, but is fundamental to the shock process. J. N. Johnson[21] at Los Alamos attributes this quasi-elastic response to the accumulation of internal stresses created by the shock process. Specific internal stress models were investigated and then compared to experimental data to arrive at an appropriate dislocation dynamics model.

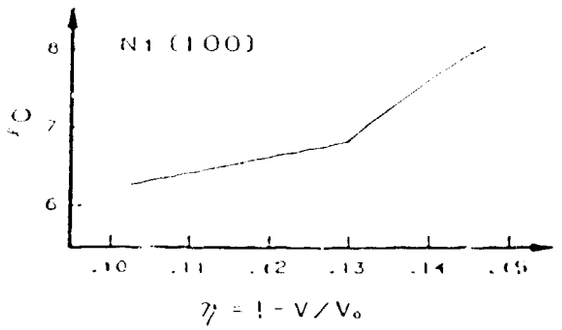

Fig. 10. Lagrangian release velocity for [100] single-crystal experiment shown in Fig. 9.

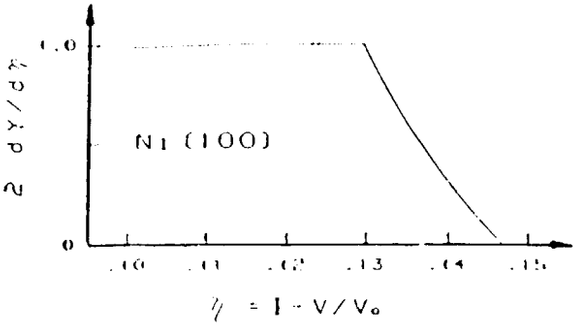

Fig. 11. Ratio of plastic to total strain increment for release wave profile shown in Fig. 10.

HUGONIOTS OF POLYSTYRENE FOAMS

Polystyrene (PS) foams can be used as low-impedance standards to measure expanded release states in high explosives and other materials of interest. Previous PS foam Hugoniots[6] used the IM technique to determine particle velocities. There is some concern about these measurements because of the uncertainties in the flash-gap transit time corrections and also the ability to accurately calculate IM match solutions of highly expanded states. The previous foam data also had a relatively large density variation for a given nominal density.

PS samples were fabricated by cold pressing commercial PS foam and subsequently slowly heating to approximately 90° C. The samples were held at this temperature for about ten hours and then allowed to cool to room temperature. The samples were homogenous flat discs that could be machined to tolerances suitable for accurate shock-wave measurements. Densities of these discs ranged from 0.04 to 0.5 g/cm^3. From a 165-mm-diam disc, several shock-wave samples could be fabricated with the same density.

The experimental assembly used to make these Hugoniot measurements is shown in Fig. 12. Five foam samples of various densities and a 6061Al sample, made from the same material as the impactor, were put on a shot assembly. Opaque tape was put on the back of the foam samples to block out the radiation from the hot-shocked samples and also to serve as a shim. With this geometry there are no flash-gap corrections, because all gap closure times are identical. The samples are attached to the flash block with tape that has adhesive backing on both sides. This double-backed tape is put only on the edges of the samples so that Ar gas can flow in the flash gaps. Since grooves are machined into the samples, the transit times measured are related to the difference in transit times between the shock velocity in the sample and the impactor velocity in the groove. From the 6061Al sample the impactor velocity can be determined, because its EOS is known. This assembly addresses all of the concerns previously mentioned, mainly the uncertainties in gap-closure times and the use of the IM technique to determine particle velocities in highly-expanded states. In this experiment the particle velocities are determined in the P-u_p plane by the intersection of the $P = (\rho_o u_s)u_p$ curve representing possible shock states in the sample with the 6061Al Hugoniot centered at the impactor velocity.

The Hugoniots for 0.18-g/cm^3-density PS foam is shown in Fig. 13 or Fig. 14. It is evident that this linear u_s-u_p curve passes through the origin. Consequently, its Hugoniot is given by

$$u_s = s\,u_p \quad . \tag{27}$$

The sample compression can be calculated using Eq. (19).

$$V/V_o = 1 - 1/s \tag{28}$$

Equation (28) indicates that all the states on the Hugoniot are compressed to the same asymptote volume. This is a consequence of the functional form of Eq. (27). Since these states are all at the same

volume Fig. (14), the Hugoniot energy Eq. (7) and the Mie-Grüneisen EOS, Eq. (12), can be used to determine γ for these high-temperature shock-compressed states.

$$\gamma = 2(s - 1) \tag{29}$$

The Hugoniots for PS foams with initial densities of 0.10, 0.18, and 0.36 g/cm^3 were measured. Their respective slopes were 1.11, 1.20, and 1.35. Using Eq. (28) their respective asymptote volumes are 1.00, 0.92, and 0.71 cm^3/g. Similarly, the γ's given by Eq. (29) at these asymptotic volumes are respectively 0.22, 0.39, and 0.69.

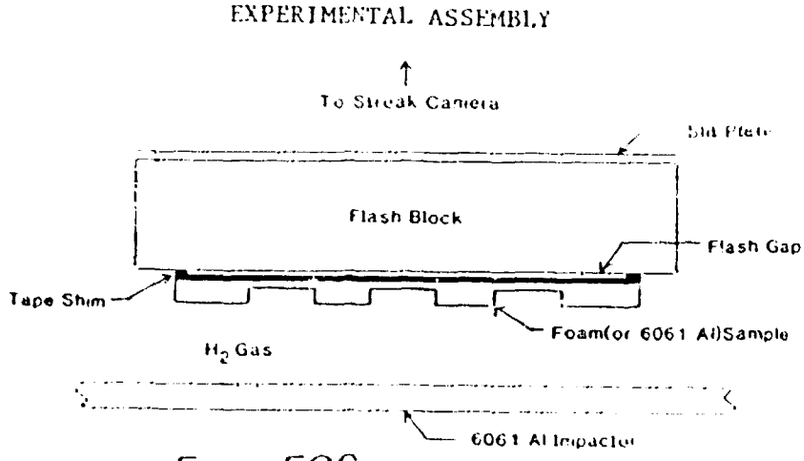

Fig. 12. PS foam EOS assembly for direct measurement of shock and impactor velocity.

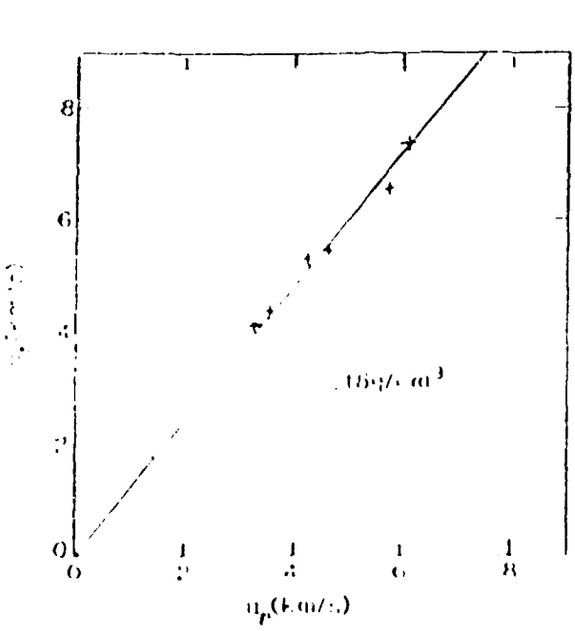

Fig. 13. u_s-u_1 Hugoniot for 0.18-g/cm^3 PS foam

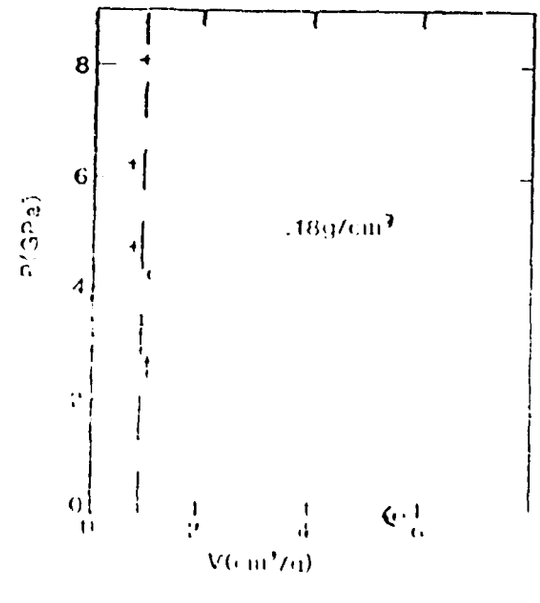

Fig. 14. P-V Hugoniot for 0.18-g/cm^3 PS foam

The increasing asymptotic volumes, with increasing porosity samples, is due to the larger increase in internal energy with the more porous samples. The thermal vibration energy is retarding sample compression. For the most porous samples (0.10 g/cm^3) the asymptotic volume 1.00 cm^3/g is greater than the ambient volume 0.956 cm^3/g (ρ_o = 1.046 g/cm^3) of fully-dense polystyrene.[6] There is a large temperature increase with pressure for these porous samples. The fact that the compression is an

isochoric (constant volume) process indicates γ is temperature independent, e.g., Eq. (29). This was true for all the porous samples studied. The γ dependence of the PS forms is different than what was observed for the porous Cu, Fe, and 2024Al studies. The asymptotic gammas are increasing with decreasing volume. The Hugoniot for the 0.10-g/cm^3 density foam, which has the highest internal energies (temperatures), has the lowest γ (0.22). This γ value is below that of a mono-atomic ideal gas, which is 2/3. This suggests other energy channels exist that prevent all the internal energy from going into thermal vibration energy, such as molecular dissociation.

ACKNOWLEDGEMENTS

I am pleased to thank R. G. McQueen for many useful discussions and for sharing his review article with me before publication. I would also like to thank J. N. Fritz for several valuable discussions and J. N. Johnson for his manuscript on quasi-elastic release modeling before publication.

REFERENCES

1. J. W. Taylor, *Shock Waves in Condensed Matter—1983*, J. R. Asay, R. A. Graham, and G. K. Straub, Eds. (North-Holland, Amsterdam, 1984), p. 3.
2. J. M. Walsh and R. H. Christian, *Phys. Rev.* **97**, No. 6, 1544 (1955).
3. J. M. Walsh, M. H. Rice, R. G. McQueen, and F. L. Yarger, *Phys. Rev.* **108**, No. 2, 196 (1957).
4. E. Grüneisen, *Ann. Phys. Berlin* **39**, 257 (1912).
5. M. H. Rice, R. G. McQueen, and J. M. Walsh, *Solid State Physics*, (Academic Press, Inc., New York, 1958), Vol. 6, p. 1.
6. S. P. Marsh, *LASL Shock Hugoniot Data* (University of California Press, Berkeley, Los Angeles, London, 1980).
7. R. G. Shreffler and W. E. Deal, *J. Appl. Phys.* **24**, No. 1, 44 (1953).
8. R. G. McQueen and S. P. Marsh, *J. Appl. Phys.* **31**, No. 7, 1253 (1960).
9. R. G. McQueen, S. P. Marsh, and W. J. Carter, *Behavior of Dense Media Under High Dynamic Pressures* (Gordon and Breach, New York, 1968), p. 67.
10. R. G. McQueen, S. P. Marsh, J. W. Taylor, J. N. Fritz, and W. J. Carter, *High Velocity Impact Phenomena*, R. Kinslow, Ed. (Academic Press, New York, 1970), p. 293.
11. R. G. McQueen, *Lecture Notes for the Enrico Fermi School of Physics*, Varenna, Italy (1989).
12. R. G. McQueen, J. W. Hopson, and J. N. Fritz, *Rev. Sci. Instrum.* **53**, No. 2, 245 (1982).
13. C. Beck, *Rev. Sci. Instrum.* **47**, No. 5, 537 (1976).
14. A. L. Ruoff, *J. Appl. Phys.* **38**, No. 13, 4976 (1967).
15. D. C. Wallace, *Thermodynamics of Crystals*, (Wiley, New York, 1972), p. 5.
16. C. E. Morris, J. N. Fritz, and R. G. McQueen, *J. Chem. Phys.* **80**, No. 10, 5203 (1984).
17. R. Jeanloz and R. Grover, *Shock Waves in Condensed Matter—1987*, S. C. Schmidt and N. C. Holmes, Eds. (North Holland, Amsterdam, 1988), p. 69.
18. G. T. Gray III, *Shock Waves in Condensed Matter—1989*, S. C. Schmidt, J. N. Johnson, and L. W. Davison, Eds. (Elsevier Science Publishers B.V., 1990), p. 407.
19. J. R. Asay and L. C. Chhabildas, *Shock Waves and High Strain Rate Phenomena in Metals—1981*, M. A. Meyers and L. A. Murr, Eds. (Plenum Publishing Corp., New York, 1981) p. 417.
20. J. W. Taylor, *J. Appl. Phys.* **36**, No. 10, 3146 (1965).
21. J. N. Johnson, P. S. Lomdahl, and J. M. Will, "Analysis of Internal Stress in the Shock Compressed State From Unloading Wave Data," in preparation (November 1990).